Fusion Engineering and Design 96–97 (2015) 659–663

Contents lists available at ScienceDirect

Fusion Engineering and Design

journal homepage: www.elsevier.com/locate/fusengdes

Three-dimensional analysis of JT-60SA conducting structures in view of RWM control

S. Mastrostefano[a,*], P. Bettini[b,c], T. Bolzonella[b], M. Furno Palumbo[b,c], Y.Q. Liu[d], G. Matsunaga[e], R. Specogna[f], M. Takechi[e], F. Villone[a]

[a] Consorzio CREATE, DIEI, Università di Cassino e del Lazio Meridionale, Cassino, FR, Italy
[b] Consorzio RFX, Padova, Italy
[c] DII, Università di Padova, Padova, Italy
[d] CCFE Fusion Association, Culham Science Centre, Abingdon OX14 3DB, UK
[e] Japan Atomic Energy Agency, Naka, Ibaraki 311-0193, Japan
[f] DIEGM, Università di Udine, Udine, Italy

HIGHLIGHTS

- 3D electromagnetic modelling of the JT60-SA tokamak has been carried out.
- Frequency-domain electromagnetic characterization of active coils has been achieved.
- Plasma response has been included so as to self-consistently study resistive wall modes with 3D conductors.

ARTICLE INFO

Article history:
Received 3 October 2014
Received in revised form 14 May 2015
Accepted 21 May 2015

Keywords:
Magnetohydrodynamics (MHD)
Resistive wall modes (RWM)
3D modeling

ABSTRACT

This paper reports the results of detailed 3D modelling of the JT60-SA tokamak. Different computational tools have been used, ranging from a purely electromagnetic description to models including the plasma response. Detailed 3D finite elements meshes have been developed, including key conducting structures of JT60-SA. The positive comparison of results produced with different assumptions and independent codes increases confidence in results. Frequency-domain electromagnetic characterization of active coils has been achieved, as well as resistive wall modes growth rate computation.

1. Introduction

The JT-60SA experiment [1,2] is a large (major radius R∼3m, typical aspect ratio A ∼2.5–2.6) superconducting tokamak device being built as joint international project between Japan and Europe. One of its design requirements [1] is to sustain high beta plasmas exceeding the no-wall ideal stability limits. In order to help the feedback control of MHD instabilities in this scenario – in particular the so-called resistive wall modes (RWMs) – 18 internal active coils are foreseen, together with a double-wall conducting shell for passive stabilization.

In the presence of active coils covering only partially the outer surface of the plasma, MHD control inherently involves 3D aspects and couplings, as already demonstrated by experiments in other devices exploring the effect of different geometries of active coils (see e.g. [3]). The analyses that follow are intended to complement in this direction previous 2D studies [4] and aim at progressing towards a quantitative description of the feedback coil action together with the stabilizing effect of the passive structures.

This work presents the 3D electromagnetic numerical analysis of active and passive conducting structures of JT-60SA which are relevant for RWM stability and control. This is carried out with several different codes (CAFE [5], CARIDDI [6] and CarMa [7]), in order to gain confidence in the results. The final aim is to get to an overall 3D model of the system which includes the plasma response [7]. After presenting the numerical framework and the device models adopted, results from the vacuum application of external fields are compared. Finally, RWM stability properties for an equilibrium representative of one of the JT-60SA target scenarios are outlined to add some insight on the potentials of this approach.

* Corresponding author.
E-mail address: s.mastrostefano@unicas.it (S. Mastrostefano).

http://dx.doi.org/10.1016/j.fusengdes.2015.05.045
0920-3796/

2. Numerical models

2.1. Electromagnetic models

Two different 3D electromagnetic codes (CAFE, CARIDDI) have been successfully applied to JT60-SA, allowing a useful cross-check and validation.

CAFE uses a discrete geometric formulation based on the reduced magnetic vector potential [9] over a mesh made of hexahedral elements. Incidence matrix $\underline{\underline{C}}$ stores the incidence between face–edge pairs [10]. The discrete formulation needs also the dual complex whose incidences between dual face–dual edge pairs are stored in the matrix $\underline{\underline{C}}^T$ [10]. By combining the discrete Ampère's and Faraday's laws, in frequency domain, with the discrete counterpart of the constitutive laws for the magnetic flux density **B** and the current density **J**, a symmetric complex linear system of equations is obtained:

$$(\underline{\underline{C}}^T \underline{\underline{\nu}} \underline{\underline{C}} + i\omega \underline{\underline{\sigma}}) \underline{A}_r = -i\omega \underline{\underline{\sigma}} \underline{A}_s \tag{1}$$

where $\underline{A}_r$ is the contribution to the line integration of the magnetic vector potential of the reaction field (due to the eddy currents induced in the conducting regions only), $\underline{\underline{\nu}}$, $\underline{\underline{\sigma}}$ are material dependent square matrices and ω is the angular frequency. Each entry of $\underline{A}_s$ in the RHS of (1), representing the line integration of the magnetic vector potential produced by the sources (active coils), is computed in the conducting regions with standard closed formulas (Biot–Savart law) and is zero otherwise. The main advantage of this formulation is that (1) is very sparse (non-zero entries are approx. 5% regardless of the dimension/fineness of the grid) and can be solved efficiently with a direct solver and a standard *tree-cotree gauge* up to some millions of unknowns, enabling the use of the finest meshes for the conducting regions, accounting for many details impractical for integral formulations. The main disadvantage is related to the additional effort required to produce the mesh also of air/vacuum (plasma included) regions.

CARIDDI is based on an integral formulation of the eddy currents problem in non-magnetic conductors V_c. The electric field **E** is given by (**A** is the magnetic vector potential, φ is the electric scalar potential):

$$\mathbf{E} = -\frac{\partial \mathbf{A}}{\partial t} - \nabla\phi \tag{2}$$

Ohm's law in weak form becomes:

$$\int_{V_c} \eta \mathbf{J} \cdot \mathbf{w}\, dV + \frac{\partial}{\partial t} \int_{V_c} \mathbf{A} \cdot \mathbf{w}\, dV + \int_{V_c} \nabla\phi \cdot \mathbf{w}\, dV = 0 \tag{3}$$

where **w** is a suitable test function, **J** is the current density and η is the resistivity. The solenoidality of the current density is guaranteed thanks to the electric vector potential **T** (such that $\mathbf{J} = \nabla \times \mathbf{T}$) [6]. From the numerical point of view, we give a finite elements discretization of V_c; **T** is expanded in terms of edge elements $\mathbf{N}_k$:

$$\mathbf{T} = \sum_k I_k \mathbf{N}_k \Rightarrow \mathbf{J} = \sum_k I_k \nabla \times \mathbf{N}_k \tag{4}$$

Solving (3) with the Galerkin method, where **A** is computed from **J** via Biot–Savart law, we have:

$$\underline{\underline{L}} \frac{d\underline{I}}{dt} + \underline{\underline{R}} \underline{I} = \underline{V} \tag{5}$$

$$L_{i,j} = \frac{\mu_0}{4\pi} \int_{V_c} \int_{V_c} \frac{\nabla \times \mathbf{N}_i(\underline{r}) \cdot \nabla \times \mathbf{N}_j(\underline{r}')}{|\underline{r} - \underline{r}'|} dV dV' \tag{6}$$

$$R_{i,j} = \int_{V_c} \nabla \times \mathbf{N}_i \cdot \eta \cdot \nabla \times \mathbf{N}_j dV \tag{7}$$

where $\underline{I}$ is the vector of degrees of freedom (DoF) I_k defined in (4) and $\underline{V}$ is the vector of externally applied voltages across electrodes. The main advantage of this numerical approach is that a mesh only of the conducting domain is needed. Moreover, the formulation can be coupled to a plasma response [6], as in the CarMa code briefly discussed in the following. The main disadvantages are the storage and inversion of fully populated matrices due to volume integral formulation.

2.2. Plasma model: CarMa code

When also the plasma is present, a term must be added to (5) [11]:

$$\underline{\underline{L}} \frac{d\underline{I}}{dt} + \underline{\underline{R}} \underline{I} + \frac{d\underline{U}}{dt} = \underline{V} \tag{8}$$

$$U_i = \int_{V_c} \nabla \times \mathbf{N}_i \cdot \mathbf{A}_p\, dV \tag{9}$$

where $\mathbf{A}_p$ is the magnetic vector potential due to plasma currents. In order to compute this term, a suitable coupling surface Σ is introduced, in between the plasma and the conducting structures. The plasma response matrix $\underline{\underline{S}}$ is calculated with the MARS-F code [12], solving linearized MHD equations inside Σ for unit magnetic field perturbations on Σ. The resulting is called CarMa code, being a combination of CARIDDI for eddy currents computation and of MARS-F for MHD solution.

The magnetic field on Σ due to external structures is computed as $\underline{\underline{Q}}\underline{I}$, where $\underline{\underline{Q}}$ is the Biot–Savart matrix. The magnetic field on the structures due to the plasma is calculated via equivalent surface currents located on Σ, which are taken into account via a suitable mutual impedance matrix $\underline{\underline{M}}$. To sum up, the plasma term (9) can be expressed as $\underline{U} = \underline{\underline{MSQ}}\underline{I}$, so that (8) becomes, with obvious redefinitions:

$$\underline{\underline{L}}^* \frac{d\underline{I}}{dt} + \underline{\underline{R}} \underline{I} = \underline{V} \tag{10}$$

System (10) can be easily recast in standard state space form. The dynamical matrix $-(\underline{\underline{L}}^*)^{-1}\underline{\underline{R}}$ shows some unstable eigenvalues, which are the growth rates of the RWM in presence of volumetric 3D structures [13].

3. JT60-SA geometry and model

One of the missions of JT-60SA is to pursue non-inductive steady-state operations with values of the plasma pressure exceeding the no-wall ideal MHD stability limits. Consequently, effective MHD control system tools have to be implemented in the device, including RWM control system. Starting from a CAD description of JT60-SA, a fully hexahedral mesh has been obtained. The main difficulty of 3D modelling of the machine (both CAD and mesh generation) is represented by the lack of symmetry of the conducting structures (see Fig. 1).

The structures considered in the present analysis are:

- The stabilizing plate (SP): composed of two shells with stiffening ribs,[1] all made of stainless steel SS316. It presents several holes for diagnostics vacuum and external heating systems.
- The vacuum vessel (VV): made of stainless steel, includes ports and stiffening ribs. In this study it is modelled without holes.

[1] Presently the SP is modelled in CARIDDI without stiffening ribs; an anisotropic equivalent resistivity can be adopted.

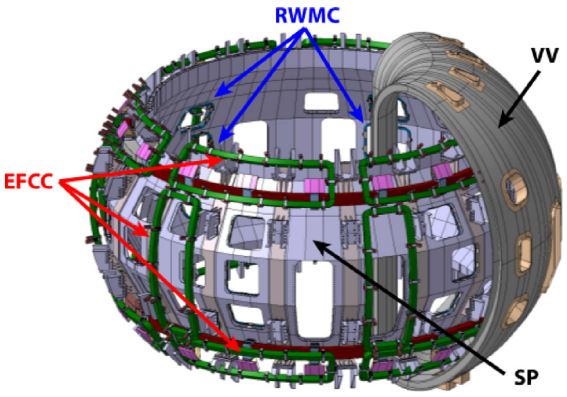

Fig. 1. JT-60SA. The control coils (RWMC, EFCC) are shown together with the stabilizing plate (SP) and the vacuum vessel (VV). [JT-60SA Research Plan, ver. 3.1].

- The resistive wall mode coils (RWMC): 3-poloidal × 6-toroidal coils, installed on the SP inner side, for active stabilization against plasma instabilities.
- The error field correction coils (EFCC): 3-poloidal × 6-toroidal coils, placed in between SP and VV, complement the control system.

4. Results

4.1. Electromagnetic models

A simplified geometry, with symmetric conducting structures (generated by rotation of a 20° symmetry cell), is introduced to allow a reliable cross-check of the results between the numerical codes and an easier evaluation of the effects of some parts of the machine.

One out of 6 equatorial RWM coil has been fed with AC current at different frequencies (10, 100, 1000 Hz); the resulting magnetic field (radial component) has been computed on a 40 × 40 grid placed before the coil on the plasma side (see Fig. 2). The 2D map of the radial field (real, imaginary components, 100 Hz) is shown in Fig. 3.

Both codes have been first run with the same geometry (SP w/o the stiffening ribs): the results are in excellent agreement. Then a comparison between two different models (SP with stiffening ribs (CAFE) and w/o stiffening ribs (CARIDDI)) has been carried out to highlight the influence of this specific detail in the behaviour of the overall system in the frequency domain. In Fig. 4 a comparison is shown, in terms of radial field along the central line of the grid

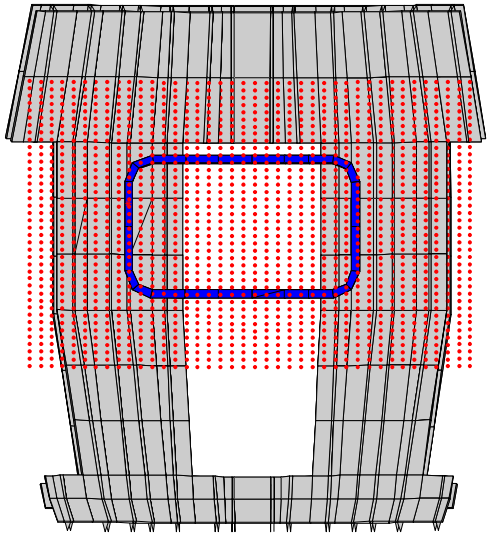

Fig. 2. A detail of the SP implemented in the symmetric geometry for CAFE (stiffening ribs are included), together with a RWM coil and the grid of points used for field calculations.

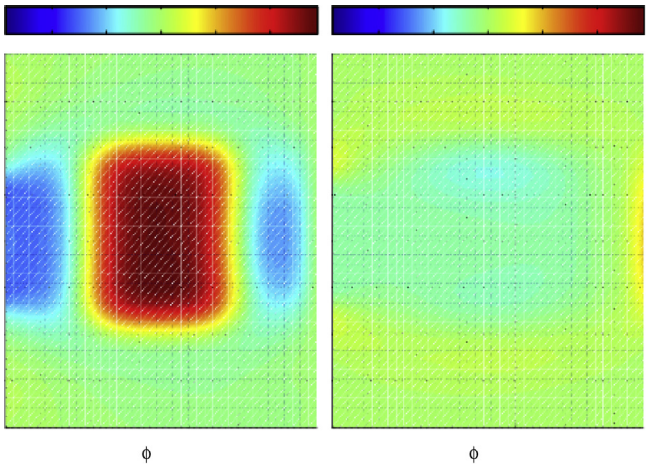

Fig. 3. 2D map (rectified view along toroidal and vertical directions) of the real (left) and imaginary (right) components of the radial field (towards *z*-axis) at 100 Hz, arbitrary units.

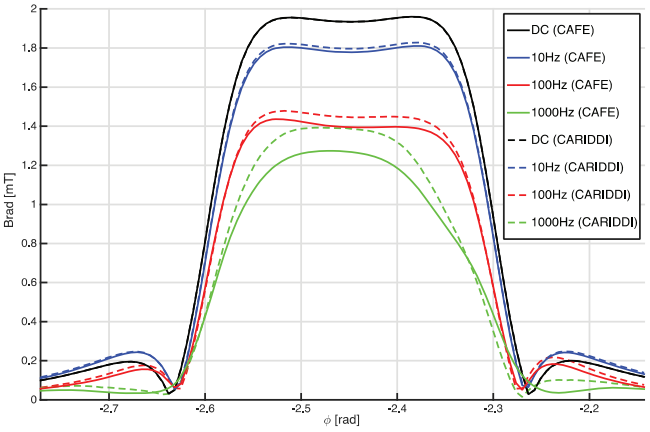

Fig. 4. Magnetic field amplitude (radial component) computed from DC to 1 kHz in a subset of the gridpoints shown in Fig. 2 (horizontal line at $z = 0$ m, $\Delta\varphi = \pm 10°$).

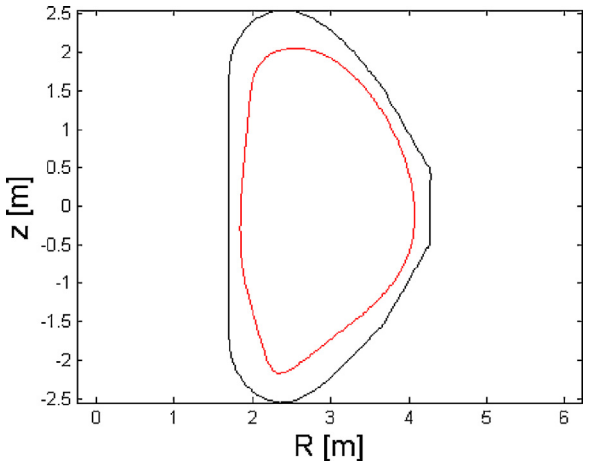

Fig. 5. Plasma boundary and poloidal trace of the 2D continuous wall located at the stabilizing plate.

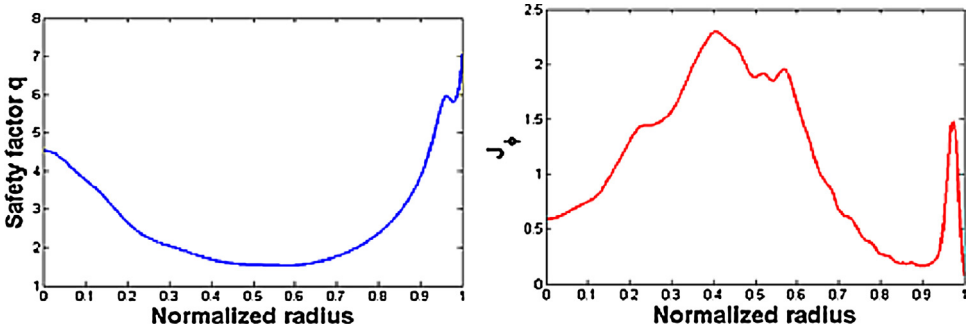

Fig. 6. Safety factor and toroidal current profiles.

($z = 0$ m, $\Delta\varphi = \pm 10^\circ$). A fairly good agreement is found in the full frequency range: a small discrepancy is visible at the highest frequencies (4% at 100 Hz, below 10% at 1 kHz), showing up the effects of a different level of details adopted to model the conducting structures. Further details can be found in [8].

4.2. Plasma model

Fig. 5 shows the shape of the plasma boundary of the reference equilibrium. Fig. 6 shows the toroidal current density and the q profile.

The plasma current is 2.3 MA and the normalized beta is 4.26. The plasma response matrix is computed for this configuration with the MARS-F code.

A validation of the model has been carried out in 2D cases with MARS-F code itself, which can treat axisymmetric thin walls. For this reason, a 3D mesh has been considered in CarMa which mimics such thin wall, placed at the poloidal location of the stabilizing plate as in Fig. 5.

We compare in this case the results obtained by MARS-F and CarMa: both codes predict an $n = 1$ unstable mode, with a growth rate γ normalized to $n = 1$ wall time constant ($\tau_w = 87.3$ ms) equal to 6.23 for MARS-F and 6.05 for CarMa (discrepancy smaller than 3%). Fig. 7 shows the spatial pattern of current density, as computed by CarMa, corresponding to the unstable mode, with a clear $n = 1$ behaviour.

When applying the same procedure to the detailed 3D mesh described above, again a $n = 1$ unstable mode appears, with a normalized growth rate greater than 100. The normalization time constant is that of the $n = 1$ current density pattern ($\tau_w = 87.3$ ms). There is no obvious link to the frequency reported in Fig. 4, which refers to localized current density patterns. This high value of normalized growth rate is due to the fact that the stabilizing plate has

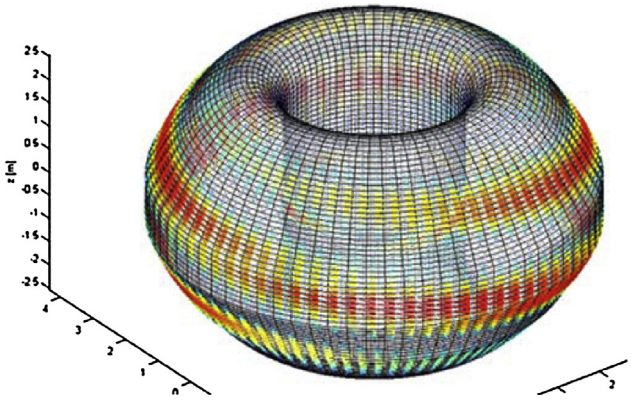

Fig. 7. 3D view of the current density pattern corresponding to the unstable eigenmode.

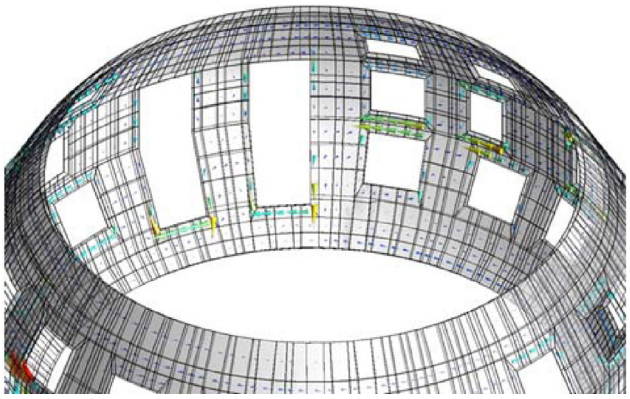

Fig. 8. Detail of the current density in the stabilizing plate.

a limited poloidal extension and has several holes, while the vessel is relatively far from the plasma. In other words, the passive stabilization of the mode is rather ineffective, so that a substantial effort of the active stabilization system could be required. An assessment will be carried out as future work.

Fig. 8 shows a detail of the spatial current density pattern of the unstable mode in the stabilizing plate. This figure confirms that the huge holes of the SP have a strong adverse effect on the stabilizing induced current, hence justifying the rather high growth rate value.

5. Conclusions

A detailed electromagnetic 3D modeling of JT60-SA has been developed, including the setup of a set of finite elements meshes that have been used by several different codes to achieve a reliable and accurate modeling of this device. Purely electromagnetic analyses have been carried out, allowing the frequency domain characterization of the RWM coils. In the future, also comparisons with commercial codes will be done.

Also plasma modelling has been pursued, which allowed the computation of the $n = 1$ RWM growth rate with various different assumptions. The next step is to use the state-space model, including the plasma response, in RWM feedback controller design and performance evaluation.

Acknowledgments

This work has been carried out within the framework of the EUROfusion Consortium and has received funding from the EU's Horizon 2020 Research and Innovation Programme under grant agreement number 633053. The views and opinions expressed herein do not necessarily reflect those of the European Commission.

This work was partially supported by the Italian MIUR under PRIN grant 2010SPS9B3.

References

[1] S. Ishida, P. Barabaschi, Y. Kamada, JT-60SA Team, Overview of the JT-60SA project, Nucl. Fusion 51 (2011) 094018.
[2] Y. Kamada, et al., Plasma regimes and research goals of JT-60SA towards ITER and DEMO, Nucl. Fusion 51 (2011) 073011.
[3] M. Baruzzo, et al., Nucl. Fusion 52 (2012) 103001.
[4] A. Ferro, et al., Studies on the requirements of the Power Supply system for the Resistive-Wall-Mode control in JT-60SA, Fusion Eng. Des. 88 (2013) 1509.
[5] P. Bettini, et al., Calculation of 3D magnetic fields produced by MHD active control systems in fusion devices, IEEE Trans. Magn. 50 (2014) 7000904.
[6] R. Albanese, G. Rubinacci, Integral formulation for 3D eddy current computation using edge elements, IEE Proc. 135A (5) (1988) 457.
[7] F. Villone, et al., Phys. Rev. Lett. 100 (2008) 255005.
[8] P. Bettini, et al., Advanced computational tools for the characterization of the dynamic response of MHD control systems in large fusion devices, IEEE Trans. Magn. (2015), http://dx.doi.org/10.1109/TMAG.2014.2360158
[9] O. Bíró, Edge element formulations of eddy current problems, Comput. Methods Appl. Mech. Eng. 169 (1999) 391–405.
[10] E. Tonti, The Mathematical Structure of Classical and Relativistic Physics, Birkhauser, Basel, 2013.
[11] A. Portone, F. Villone, Y. Liu, R. Albanese, G. Rubinacci, Plasma Phys. Control. Fusion 50 (2008) 085004.
[12] Y.Q. Liu, A. Bondeson, C.M. Fransson, B. Lennartson, C. Breitholtz, Phys. Plasmas 7 (2000) 3681.
[13] F. Villone, et al., Nucl. Fusion 50 (2010) 125011.